Energy 231 (2021) 120695

Contents lists available at ScienceDirect

Energy

journal homepage: www.elsevier.com/locate/energy

Framework for energy storage selection to design the next generation of electrified military vehicles

Edoardo Catenaro [a], Denise M. Rizzo [b], Simona Onori [a, *]

[a] Department of Energy Resource Engineering, Stanford University, 367 Panama St, Stanford, CA, 94305, USA
[b] U.S. Army CCDC Ground Vehicle Systems Center, 6501 E. 11 Mile Road, Warren, MI, 48397, USA

ARTICLE INFO

Article history:
Received 19 June 2020
Received in revised form
19 February 2021
Accepted 19 April 2021
Available online 6 May 2021

Keywords:
Lithium-ion battery
Supercapacitor
Enhanced-ragone plot
Military ground vehicles
Energy storage selection

ABSTRACT

In this paper, a methodology is proposed that aims at selecting the most suitable energy storage system (ESS) for a targeted application. Specifically, the focus is on electrified military vehicles for the wide range of load requirements, driving missions and operating conditions call for such a cohesive framework. The method uses the Enhanced-Ragone plot (ERp) as a guiding tool to map the performance of different lithium-ion batteries, as a function of C-rate and temperature, and supercapacitors, on the specific power and specific energy log-log plane. A frequency-based segmentation strategy is employed to assign the requested power to the powertrain actuators. Both full-electric battery-powered and hybrid electric vehicle (including an internal combustion engine, battery and supercapacitors) configurations are considered. Using the ERp, ESSs that are able to match the C-rate corresponding to the power-to-energy ratio calculated from the load are selected. Moreover, weight, volume, number of cells and pack energy of the selected ESSs are also returned from the design framework. The algorithm is tested over three vehicle powertrains which strongly differ in load requirements - Tesla Model S, Tesla Semi truck and high-mobility multipurpose wheeled vehicle.

1. Introduction

Advancements in energy storage systems (ESSs), such as lithium-ion batteries (LIBs), are enabling the wide spread of electrified vehicles on the road [1]. The deployment of electric vehicles (EVs) and hybrid electric vehicles (HEVs) has seen a significant rise over the past decade [2].

In military applications, hybridization and/or electrification of the powertrain can provide increased tactical capability of military vehicles by increasing the available on-board power, along with reducing the battlefield fuel costs [3]. Past data and future projections point out the constantly increasing battlefield fuel cost that can be as high as $100\$/L$ due to higher cost of the power propulsion systems, new on-board monitoring equipment and large fuel convoys. The adoption of electrified drivetrains would result in the optimization of fuel consumption based on the optimal operation of the engine and ESS along with benefits derived from brake energy recovery. Furthermore, during the electric-only mode, noise and thermal signatures can be significantly reduced [3]. Finally, reducing reliance on fuel would limit the transport of fuel from refinery sites to the locations where troops operate, thus lessening hazardous exposure to enemy ambushes which could cost human lives [4].

Electrification of the military vehicle fleet calls for a design strategy geared towards the optimal sizing of powertrain components while accounting for diverse load requirements, driving cycle missions, operating and geographical conditions.

Several works have addressed the optimal design of ESS (i.e. battery) in standalone and hybrid configuration - i.e. combined with supercapacitors (SCs)- for vehicle applications ranging from light-duty to heavy-duty trucks. Proposed approaches can be classified into *sequential*, *alternating* and *simultaneous* methods. Sequential strategies are also referred to as a *design-first-then-control* methodologies [5] where the ESS is designed first and the energy management problem is solved afterwards. Alternating strategies do not consider the mutual dependence between ESS and energy management strategy (EMS) design and they use an iterative process that optimizes ESS for a defined EMS, and then optimize the EMS for a given ESS [5].

Finally, the simultaneous methods acknowledge the strong

* Corresponding author.
E-mail addresses: cedoardo@stanford.edu (E. Catenaro), denise.m.rizzo2.civ@mail.mil (D.M. Rizzo), sonori@stanford.edu (S. Onori).

https://doi.org/10.1016/j.energy.2021.120695
0360-5442/

Acronyms and Symbols

ARTS	All-purpose remote transport system
BMS	Battery management system
CV	Conventional vehicle
EMS	Energy management system
ERp	Enhanced-Ragone plot
ESS	Energy storage system
EV	Electric vehicle
FMTV	Family medium tactical vehicle
HEMTT	Heavy expanded mobility tactical truck
HESS	Hybrid energy storage system
HEV	Hybrid-electric vehicle
HMMWV	High mobility multipurpose wheeled vehicle
ICE	Internal combustion engine
LFP	Iron-phosphate
LIB	Lithium-ion batteries
M-ATV	Mine-resistant ambush protected all-terrain vehicle
MV	Military vehicle
NCA	Nickel-cobalt-aluminum-oxide
NMC	Nickel-manganese-cobalt-oxide
P/E	Power-to-energy
Rp	Ragone plot
SC	Supercapacitor
TMS	Tesla Model S
TST	Tesla Semi truck
TUGV	Tactical unmanned ground vehicle

coupling between the ESS design and EMS optimization. Examples are found in Refs. [6,7] for the military series-hybrid electric truck equipped with battery pack only and battery pack and SCs, respectively.

In [8], the sizing of the powertrain components for a Plug-in Series-HEV battery-powered vehicle is optimized using convex optimization along with cost considerations. In Refs. [9,10] a series-parallel vehicle and plug-in series-HEV, respectively, equipped with three different storage systems, namely battery pack, SC pack and the combination of the two, were optimized using convex optimization.

Ragone plot (Rp) [11] has been exploited as a tool for the optimal selection of storage devices. In Ref. [12], the energy storage component, in the form of standalone battery, SC or combination of the two, is optimized for a mid-size fuel cell SUV. In Ref. [13], authors outlined an optimization routine, based on Rp, to choose between a lead-acid battery and SC. Rp is also used to select the ESS in a wind power farm [14]. In Ref. [15], Rp is used for storage system optimization based on technical and economic information.

The above studies propose an *ad-hoc* design solution based on an *a-priori* ESS or hybrid ESS (HESS) configuration without addressing the scalability aspect of the methodology. When the application under study is characterized by a wide range of load requirements or diverse missions or operating conditions, such an approach fails to provide a proper solution. This is the case of military vehicle (MV) applications. The strong variation in load requirements and functions experienced by MVs makes the energy storage selection a challenging task [3]. Moreover, the wide span of available electrified technologies (Fig. 1) shows that many are the ways to electrify the powertrain - from micro hybrid to full electric - and therefore the ESS. For instance, LIBs are the best storage technology for a plug-in hybrid vehicle whereas a lead-acid battery is the way to go for a micro hybrid [16]. Moreover, not only do MVs vary in weight, ranging from few kilograms up to few tons, as shown in Fig. 2, but they also experience very diverse environmental conditions/loads in terms of duty cycles, transient operation, road grade and ground unevenness.

The research presented in this paper aims to develop a scalable methodology to match vehicle load characteristics/requirements with the most suitable ESS — either in the form of standalone technology or hybrid configuration (for example, using LIBs together with SCs) - for improved performance across usage.

The *Enhanced-Ragone plot* (ERp), developed in Ref. [27], displays the performance of a set of LIBs in terms of their specific energy and specific power and as a function of C-rate and temP/Eperature of operation, across several cell samples. The time taken by the device to be discharged, from a fully charged state, is learned from the ERp and is proportional to the power to energy (P/E) ratio of the ESS (in the log-log plane this corresponds to diagonal lines).

In [27], the ERp is experimentally populated with data from 18650 nickel-cobalt-aluminum-oxide (NCA), 21700 nickel-manganese-cobalt-oxide (NMC) and 26650 iron-phosphate (LFP) LIB tested over a wide range of C-rate and various temperatures. Along with LIBs, the ERp also includes the performance of the

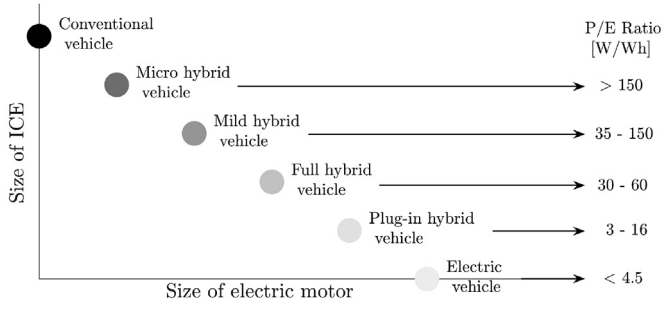

Fig. 1. Spectrum of available vehicle technologies and corresponding P/E ratio required to the ESS. The range of values is from battery specifications used in EV (i.e. Tesla Model S, Chevrolet Bolt, BMW i3 [16]), plug-in HEV (i.e. Audi A3, Chevrolet Volt, BMW i8 [16]), full hybrid (i.e. Toyota Prius3, Ford Fusion [17]), mild hybrid (i.e. Audi A8 [18], Chevrolet Malibu [19], BMW ED [17]) and micro hybrid (i.e. Citroen C3, Smart [17]).

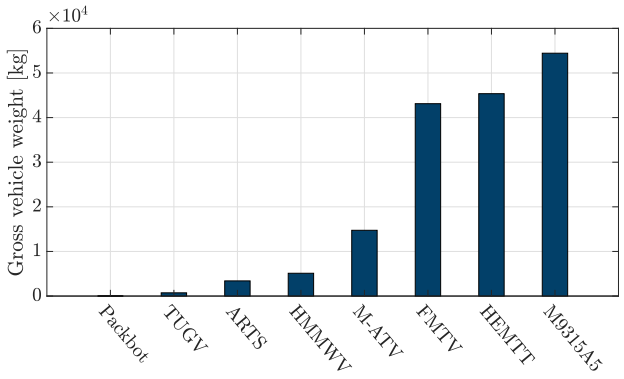

Fig. 2. Different classes of MVs by gross weight. From the left (lighter) to the right (heavier): packbot small-class robotics, tactical unmanned ground vehicle (TUGV) [20], all-purpose remote transport system (ARTS) [21], high mobility multipurpose wheeled vehicle (HMMWV) [22], mine-resistant ambush protected all-terrain vehicle (M-ATV) [23], family medium tactical vehicle (FMTV) [24], heavy expanded mobility tactical truck (HEMTT) [25] and line haul tractor M9315A5 [26].

BCAP0350 Mx SC [28].

In this work, we propose a design framework that employs the ERp as a basis to match given vehicle load characteristics with the best suitable energy storage solution (either in its standalone or hybrid configuration). The proposed design framework involves a first part where the vehicle is analyzed from a power requirement perspective (from the wheel to each actuator in the powertrain) and a second part related to the ESS selection using the ERp.

We consider a hybrid powertrain equipped with an internal combustion engine (ICE), a battery pack and SCs.

Using a vehicle backward model and starting from a known driving cycle (vehicle trace over time) and road grade profile, the power at the wheel is first calculated and then subjected to a frequency-based segmentation [29]. Low frequencies - computed by filtering the power at the wheel with a low-pass filter - are assigned to the ICE, whereas the remaining power is supplied by battery and SC. Medium frequencies are assigned to the battery whereas the high frequency power is taken up by the SC. The P/E ratio of each storage device is then calculated. To meet the power and energy requirements of the vehicle, the energy storage device must handle the C-rate corresponding to the P/E ratio calculated from the load. The matching operation returns a candidate storage technology along with the initial sizing - in terms of weight, volume, number of cells and pack energy. We validate the matching design algorithm on three vehicle powertrains, namely, Tesla Model S (TMS), Tesla Semi truck (TST) and high mobility multipurpose wheeled vehicle (HMMWV). These vehicles, which differ in load requirements, have been tested over energy (constant speed over a fixed range) and power (constant acceleration) tests, US06 and UDDS driving cycles [30], and the distance dependent grade Harford military cycle [7].

The main contributions of this paper are summarized as follows:

- Use of ERp as a design tool coupled with the frequency segmentation strategy;
- Match the P/E ratio of the powertrain components with the C-rate of operation of the storage device(s);
- Agnostic-based selection of the most suitable energy storage, along with its weight, volume, energy and number of cells;
- Test the ERp-based methodology over three vehicles - ranging in weight and mission - TMS, TST and HMMWV under different driving scenarios.

Moreover, a sensitivity analysis of key model parameters used in the matching design framework is presented.

The paper is organized as follows. A summary of the ERp is reported in Section 2. In Section 3, the overall design framework is described step-by-step. Section 4 shows the methodology applied to multiple simulation scenarios across three vehicle powertrains. Section 5 provides a brief description about safety performance. Finally, Section 6 gathers the conclusions of the proposed study.

2. Enhanced-Ragone plot

The experimental design of the ERp conducted in Ref. [27] is briefly summarized in this section. The LIBs tested to populate the ERp are[1]: 18650 $LiNiCoAlO_2$/graphite [31], 21700 $LiNiMnCoO_2$/graphite [32] and 26650 $LiFePO_4$/graphite [33], referred to as NCA, NMC and LFP, respectively. Measurements were taken over six cell samples for each chemistry. Galvanostatic discharge experiments were conducted at controlled temperature of $5^\circ C$, $25^\circ C$ and $35^\circ C$ starting from fully charged condition, i.e. 100% state-of-charge, until the cut-off voltage was reached at discharge rate x equal to:

- $C/20$, $1C$, $2C$, $3C$, $5C$ for NCA and NMC,
- $C/20$, $1C$, $2C$, $3C$, $5C$, $10C$, $15C$, $20C$ for LFP.

The experimental dataset is available in Ref. [34]. Gravimetric energy density (or specific energy) and gravimetric power density (or specific power), $w_s^b(x, T_{amb})$ and $p_s^b(x, T_{amb})$, respectively, and volumetric energy density (or energy density) and volumetric power density (or power density), $w_d^b(x, T_{amb})$ and $p_d^b(x, T_{amb})$, respectively, were calculated and averaged across six cell samples for each battery chemistry b, $b = \{\text{NCA, NMC, LFP}\}$, undergoing to a discharge rate x, and controlled at temperature T_{amb}. The gravimentric ERp is shown in Fig. 3a and the volumetric ERp is shown in Fig. 3b. The specific energy (specific power) and the energy density (power density) are related through the following relationship

$$w_s^b(x, T_{amb}) = \frac{V_{cell,B}}{M_{cell,B}}\, w_d^b(x, T_{amb}), \tag{1}$$

$$p_s^b(x, T_{amb}) = \frac{V_{cell,B}}{M_{cell,B}}\, p_d^b(x, T_{amb}), \tag{2}$$

where $V_{cell,B}$ and $M_{cell,B}$ are the battery cell nominal volume and weight, respectively.

The C-rate of operation is shown, on both ERps, by diagonal lines. In the rest of the paper, the gravimetric ERp, also inclusive of the BCAP0350 Mx SC [28], is used to develop the ESS selection strategy.

3. Energy storage selection methodology

The proposed design framework, depicted in the flow diagram in Fig. 4, first analyzes the load characteristics from the driving cycles, and then identifies the ESS device(s) through the ERp that best matches the vehicle requirements.

3.1. Step 1 - vehicle requirements

Given a specified vehicle application and desired speed profile, $\dot{x}(t)$, and road grade, $\delta(t)$, a backward simulator based on the vehicle longitudinal dynamics is used [35] to compute the power demanded at the wheel, P_W, as

$$P_W = \dot{x}\left(M_{veh}\ddot{x} + M_{veh}g\sin(\delta) + M_{veh}gf_r\cos(\delta) + \frac{1}{2}\rho_{air}A_f C_d \dot{x}^2\right), \tag{3}$$

and, by time integration, the respective energy, E_W

$$E_W = \int_0^{t_f} P_W\, dt. \tag{4}$$

In Eq. (3), M_{veh} is the vehicle curb weight,[2] g is the gravitational time constant ($9.81\ \text{m/s}^2$), f_r is the rolling friction coefficient (assumed to be constant), ρ_{air} is the air density (equal to $1\ \text{kg/m}^3$), A_f is the vehicle frontal area, C_d is the drag coefficient and in Eq. (4),

[1] The nomenclature C_c/C_a refers to the anode, C_c, and cathode, C_a, composition, respectively.

[2] Whole vehicle weight excluding passengers.

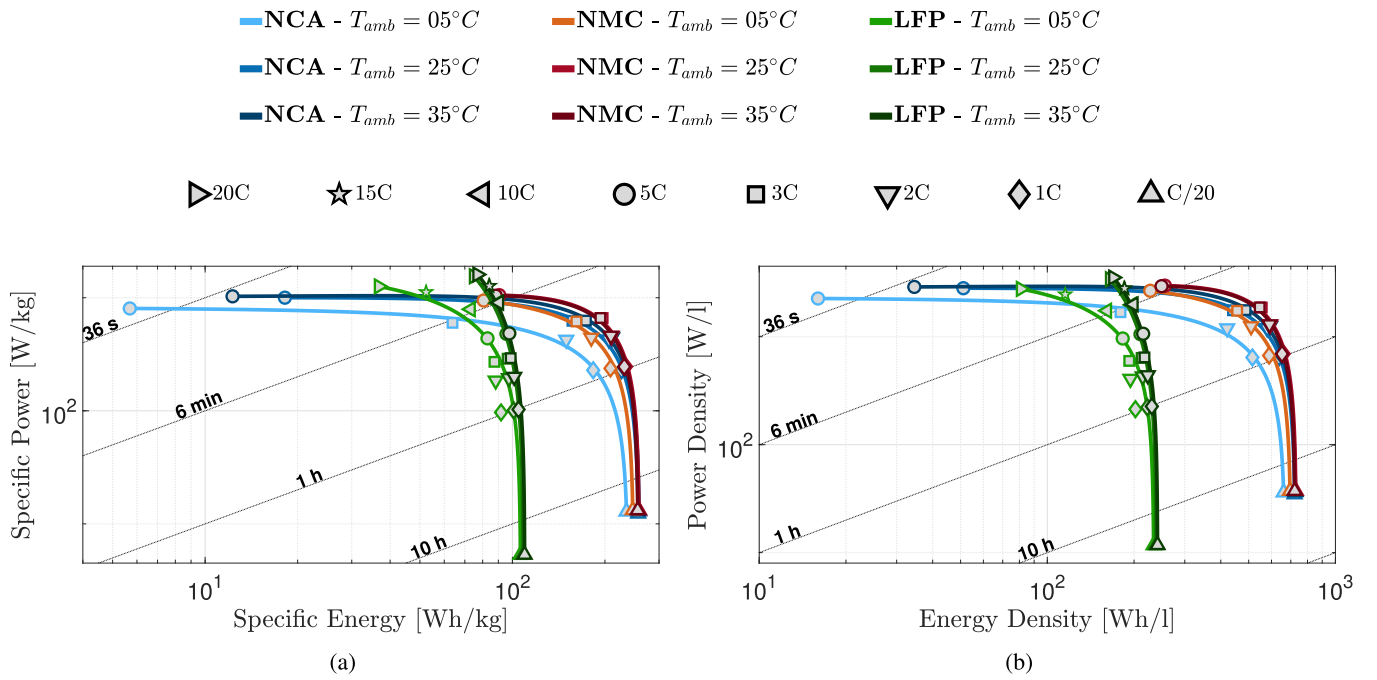

Fig. 3. Specific power versus specific energy ERp (a) and power density versus energy density ERp (b) for NCA, NMC and LFP batteries at various reference temperatures and discharge rates.

and t_f is the time duration of the driving cycle.[3] To improve equations readability, time-dependency is omitted.

A frequency-based segmentation method [29] is applied to allocate power at the wheel power, P_W, to the powertrain actuators. In particular, low frequency components are assigned to the ICE, medium frequencies to the battery and high frequencies to the SC, according to the power-split block scheme shown in Fig. 5.

Specifically, the low frequency portion of the power signal, $P_{W,l}$, is computed by filtering the power at the wheel, P_W, with a second-order low-pass filter, $F_1(s)$, with cutoff frequency $f_{cut,1}$

$$F_1(s) = \frac{1}{\left(1 + \frac{s}{2\pi f_{cut,1}}\right)^2}. \tag{5}$$

The "intermediate" power, $P_{W,int}$ - characterized by medium and high frequencies - is supplied by the battery and SC (i.e., HESS). Here, the medium frequency power component, $P_{W,m}$, is obtained by filtering $P_{W,int}$ with a second-order low-pass filter, $F_2(s)$, with cutoff frequency $f_{cut,2}$

$$F_2(s) = \frac{1}{\left(1 + \frac{s}{2\pi f_{cut,2}}\right)^2}. \tag{6}$$

The $P_{W,m}$ is assumed to be provided by the battery, whereas the high frequency signal, $P_{W,h}$, by the SC (see, Fig. 5).

The cutoff frequencies $f_{cut,1}$ and $f_{cut,2}$ are tunable parameters that determine the load on each actuator, hence defining their sizing. The cutoff frequency $f_{cut,1}$ affects the degree of vehicle electrification in that an increase of $f_{cut,1}$ leads to a larger ICE load, and consequently, a decrease of the degree of vehicle electrification whereas a decrease of $f_{cut,1}$ imposes a higher load on the HESS (i.e. battery (B) +SC) components. Asymptotically, this is summarized as follows

$$\begin{cases} \text{if } f_{cut,1} \to \infty \Rightarrow \text{CV (only ICE)} \\ \text{if } f_{cut,1} \to 0 \Rightarrow \text{EV (B + SC)} \end{cases} \tag{7}$$

where CV indicates "conventional vehicle".The cutoff frequency, $f_{cut,2}$, instead deals with the power split between the battery and SC. An increase of $f_{cut,2}$ yields to an increase of the battery load, with consequently reduction of SC load.

Table 1 reports possible vehicle configurations based on the asymptotic values of $f_{cut,1}$ and $f_{cut,2}$.

The segmented power profiles are then used to characterize the power and energy of each actuator. The battery-to-wheel powertrain efficiency for both EVs and HEVs (series and parallel configurations) - taking into account mechanical and electrical losses occurring in the battery, DC/DC converter, inverter, electric motor, transmission and differential - is approximated to 80% [36]. SCs are connected to the battery through a semi-active or fully-active configuration which introduces an electrical conversion efficiency that can be bounded to sufficiently high values [7]. Hence, we assume a fixed HESS-to-wheel powertrain efficiency, η. The power to the battery and the SC, P_B and P_{SC}, respectively, are computed as follows

$$P_B = \frac{1}{\eta} P_{W,m}, \tag{8}$$

$$P_{SC} = \frac{1}{\eta} P_{W,h}. \tag{9}$$

where positive power corresponds to discharge. For the purpose of calculating the P/E ratio during discharge, the amount of energy required to each storage device k is obtained as

[3] The initial time is always assumed equal to 0.

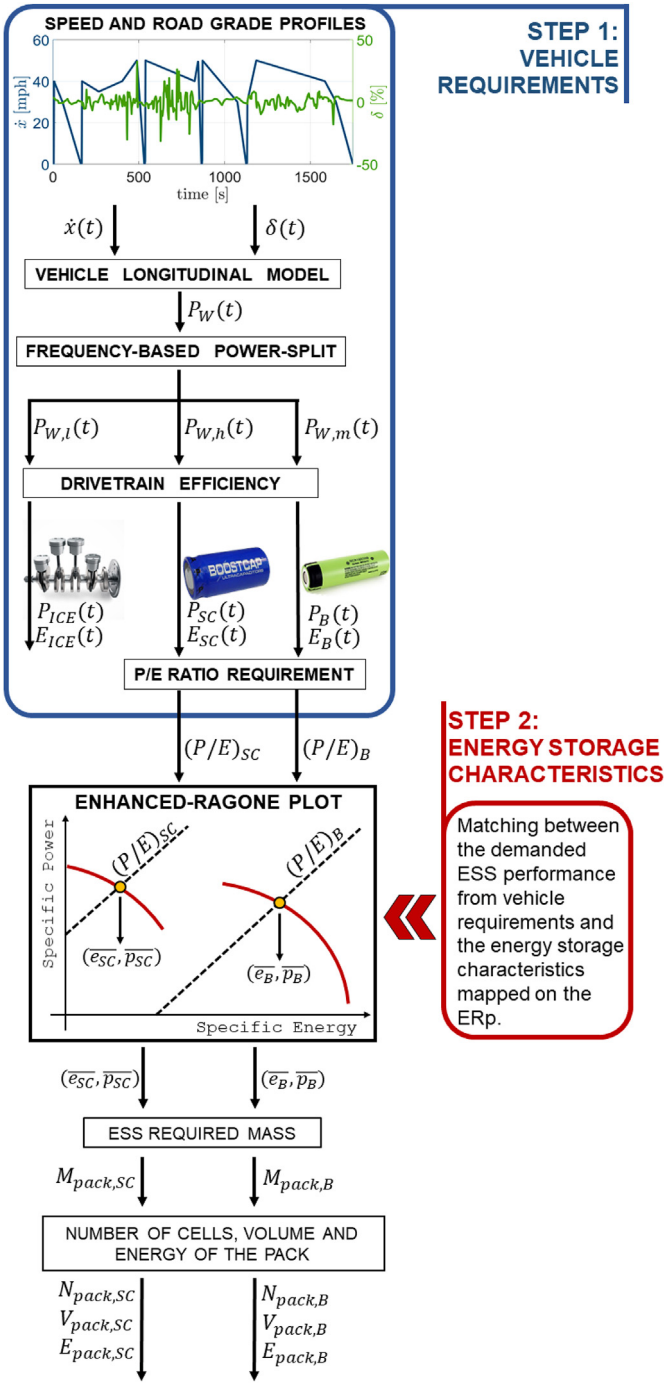

Fig. 4. Flow diagram describing the design framework composed of 1) Vehicle requirements analysis and 2) energy storage characteristics for matching strategy.

$$E_k = \int_0^{t_f} P_k \, dt \quad if \; P_k \geq 0, \quad \text{with } k = \{B, SC\}. \tag{10}$$

Finally, the P/E ratio associated to each storage device k is given as

$$(P/E)_k = \frac{\alpha P_k^*}{E_k} \quad \text{with } k = \{B, SC\}, \tag{11}$$

where P_k^* is the maximum discharge power of the storage device k

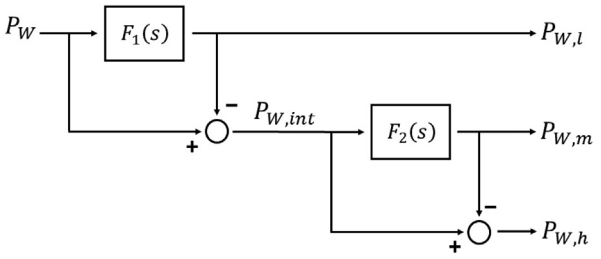

Fig. 5. Frequency-based segmentation scheme. The total power at the wheel, P_W, is segmented into low, medium and high frequency components, $P_{W,l}$, $P_{W,m}$ and $P_{W,h}$, respectively.

Table 1
Possible vehicle configurations - EV, HEV or CV - according to the choice of cutoff frequencies $f_{cut,1}$ and $f_{cut,2}$.

		$f_{cut,1}$		
		0	(0∞)	∞
$f_{cut,2}$	0	EV (SC)	HEV (ICE + SC)	CV
	(0∞)	EV (B+SC)	HEV (ICE + B + SC)	CV
	∞	EV (B)	HEV (ICE + B)	CV

and α is a weigh coefficient, assumed to be the same for the battery and SC, ranging between 0.5 and 1.

When $\alpha = 1$, the power requirements for each device correspond to their peak value, whereas, when α is modulated to assume values less than one, then the lower P/E ratio will limit the design requirements on the devices.

The upper plot of Fig. 6 shows the battery power profile for the TMS - in the battery alone configuration - over the US06 driving cycle. The time histogram of the power profile over the total driving

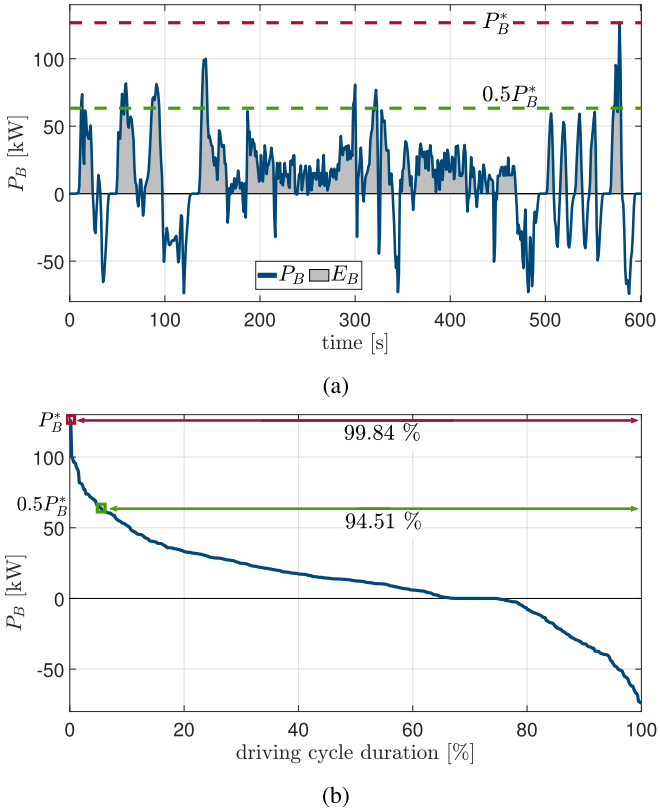

Fig. 6. (a) Demanded battery power profile and (b) respective time histogram for the TMS vehicle tested over the US06 cycle.

cycle duration expressed in percentage, is shown in the bottom plot of the same figure. As one can see, the battery power peak, P_B^*, whose value is 125.6 kW, only occurs for 0.16% of the total cycle duration. If, on one hand, sizing the battery upon the peak power value will satisfy the power demand throughout the entire cycle duration, on the other hand, it would lead to an oversized system.

By reducing α by half, the corresponding power requirement is 62.8 kW, which covers almost 95% of the total power request over the cycle duration.

The parameter α and the cutoff frequencies, $f_{cut,1}$ and $f_{cut,2}$ are being assessed through a sensitivity analysis for different driving cycles. It is worth to remark that the variation of these three parameters yields to a different sizing of the storage units, yet always satisfying the performance expected by the vehicle, both in terms of delivered power and stored energy.

The P/E ratio, computed with Eq. (11), has the unit of [1/h] and is expressed in the ERp log-log plane via the specific energy, e_k, and specific power, p_k as

$$p_k = (P/E)_k \, e_k, \quad k = \{B, SC\}. \tag{12}$$

Taking the logarithm of both sides of Eq. (12) and using Eq. (11) one gets

$$log(p_k) = log(\alpha) + log\left(\frac{P_k^*}{E_k}\right) + log(e_k), \quad k = \{B, SC\}. \tag{13}$$

Thus, the P/E ratio is represented in the ERp diagram with a series of diagonal lines, whose position in the log-log plane is shifted upward or downward according to the value assigned to α, and the ratio between power and energy requirements.

3.2. Step 2 - energy storage system characteristics

The ERp diagram is used as a tool to match the vehicle requirements with the most suitable energy storage device(s). In the ERp, the ESS performance is parametrized as a function of C-rate of discharge which is the P/E ratio of the storage device. Thus, vehicle requirements are being translated into required P/E ratios, which in turn are equivalent to the C-rates at which the device should operate to satisfy such requirements.The matching operation then consists in intersecting the characteristic curves of the devices (mapped on the ERp) and the P/E ratio lines from the vehicle and generate the point of coordinates $(\overline{e}_k \overline{p}_k)$.

The coordinates of the selected ESS candidates are used to calculate the required mass[4] of the k device as

$$M_{pack,k} = \max\left\{\frac{\alpha P_k^*}{\overline{p}_k}; \frac{E_k}{\overline{e}_k}\right\}, \quad k = \{B, SC\}. \tag{14}$$

From the calculated mass of the ESSs, one can also compute the corresponding occupied volume, $V_{pack,k}$, number of cells $N_{pack,k}$ and the overall energy of the pack, $E_{pack,k}$.

Specifically,

$$V_{pack,k} = M_{pack,k} \, \frac{V_{cell,k}}{M_{cell,k}}, \quad k = \{B, SC\}, \tag{15}$$

where $V_{cell,k}$ is the cell nominal volume and $M_{cell,k}$ is the cell nominal weight (as given by the manufacturer). From the cell nominal mass, the corresponding number of cells needed in a pack is calculated as

$$N_{pack,k} = \frac{M_{pack,k}}{M_{cell,k}}, \quad k = \{B, SC\}, \tag{16}$$

where $N_{pack,k}$ is the number of cells for device k.Furthermore, from the required mass and given the cell nominal specific energy from the manufacturer specifications, $e_{cell,k}$, the overall energy of device k, $E_{pack,k}$, is calculated as

$$E_{pack,k} = M_{pack,k} \, e_{cell,k}, \quad k = \{B, SC\}. \tag{17}$$

4. Case studies and simulation results

In this paper, three vehicles are considered (Fig. 7). The first two, manufactured by Tesla, are the TMS and the TST. The TMS has been on the market since 2012 [37], while the starting of TST production is planned by the end of 2021 [38]. These two full-electric battery-powered vehicles - whose energy storage size is known (TMS) or claimed (TST) - are used to test the proposed design framework. A comparison between the actual TMS battery pack sizing and the one returned by our framework is conducted. The analysis is then extended to the TST. Lastly, the HMMWV is considered as a test case to provide ESS design specifications.

Table 2 reports the values used for the vehicle parameters for each application. The M_{veh}, A_f and C_d for TMS are taken from Ref. [39], and for HMMWV from Ref. [22]. The TST is not on the market yet and accurate parameter values are not known. Yet, Tesla has claimed the excellent TST aerodynamic feature, in terms of drag coefficient, compared to other trucks [40] and provides a value of 0.36 for C_d. As for the vehicle mass, M_{veh}, in this paper, we consider the worst case scenario where the vehicle is in fully loaded condition [41]. Finally, for A_f we use the same value used for a set of commercialized trucks (e.g., Mercedes Actros Air, Volvo FH) [42]. Parameters f_r and η are assumed to be the same for all vehicles, whose values are taken from Refs. [35,43].

The driving profiles used in this study consist of constant speed tests over a fixed mile range (referred to as *Range* tests), constant acceleration tests (referred to as *Acc* test) and realistic driving cycle tests. For the *Range* tests, three constant speeds are used, 20, 45 and 70mph, referred to as *Range1*, *Range2* and *Range3*, respectively, over a fixed mile range of 370 miles for the TMS and HMMWV, and 500 miles for the TST. The *Acc* test is a constant acceleration from stationary condition to 60 mph over 3.7s for TMS and HMMWV, and 20s for TST. The range and acceleration performance specifications used for the TMS and TST are the ones claimed by Tesla [40,44], whereas for the HMMWV we assume the same values as for the TMS.

The US06 and UDDS (Fig. 8) are the realistic driving cycles used for the evaluation of the TMS and TST. As suggested in Ref. [16], the strict energy and power requirements derived from the US06 drive profile can be used to obtain an upper bound for battery size. Conversely, urban drive cycle - such as UDDS - can be used as a lower bound for vehicle requirements and battery sizing [45]. To provide an appropriate estimation of the size of the energy storage device for the HMMWV used in military application, the Harford cycle with distance dependent grade characteristics is used in this work (Fig. 9), [46]. The driving tests are summarized in Table 3 and the characteristics, in terms their average speed, maximum speed, average acceleration, and maximum acceleration, average road grade and maximum road grade are described in Table 4.

In the following, the case of full-electric battery-powered

[4] The computed ESS masses and volumes only consider the weight and volume of the storage devices and do not include the pack housing and other components of the pack.

(a) (b) (c)

Fig. 7. Vehicle considered in this work: (a) Tesla model S long range plus (TMS), (b) Tesla Semi truck (TST) and (c) military high mobility multipurpose wheeled vehicle (HMMWV).

Table 2
Vehicle parameter values for each application.

	TMS	HMMWV	TST
M_{veh}[kg]	2087	5112	36287.39
$A_f[m^2]$	2.34	3.58	9.7
C_d [−]	0.24	0.7	0.36
f_r [−]	0.012	0.012	0.012
η [−]	0.8	0.8	0.8

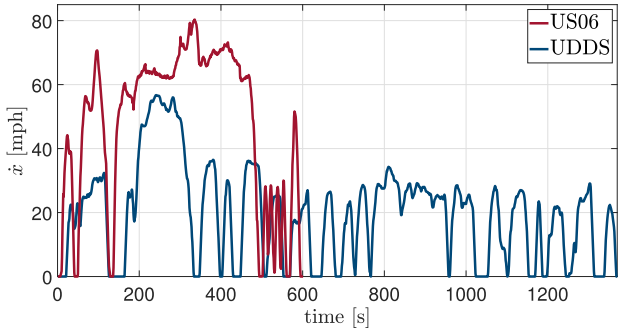

Fig. 8. US06 (red) and UDDS (blue) driving cycles. (For interpretation of the references to colour in this figure legend, the reader is referred to the Web version of this article.)

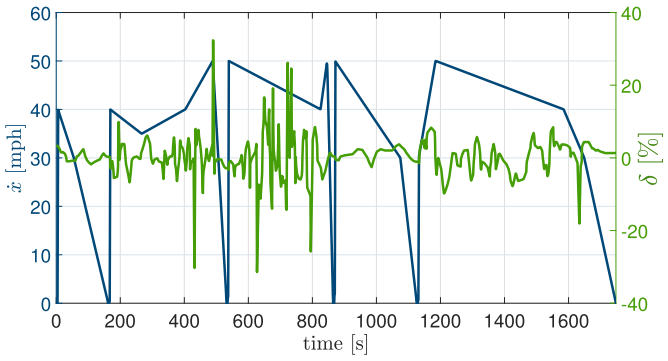

Fig. 9. Speed and road grade profile of the military Harford driving cycle.

configuration for the three vehicle applications is discussed. The hybrid configuration case follows after that.

4.1. Full-electric battery-powered configuration

In the full-electric battery-powered configuration the overall traction power comes from the battery.[5] We refer to the required P/E ratio through the notation $(P/E)_B(d,v)$, where d indicates the driving profile and v the type of vehicle application. Fig. 10 shows the ERp diagram with the $(P/E)_B(\bullet, \text{TMS})$ ratios computed for the TMS vehicle and for all driving scenarios.

The diagonal lines on the ERp provide information on the C-rate requested to the battery, *i.e.* $(P/E)_B$. As shown in Fig. 10, the less demanding cycles are, in order, *Range1*, *Range2*, and *Range3*, whose discharge rates can be handled by the three LIB chemistry. It is easy to show that, in the case of constant speed, the $(P/E)_B$ only depends on α and the duration of the cycle and not on other vehicle parameters. As the severity of the driving scenarios increases, the $(P/E)_B$ diagonal lines move upwards. All chemistry can still satisfy the specific energy and power requirements imposed by the cycles. In particular, the rates of discharge for UDDS and US06 are of 60 min and 36 min, respectively.

Driving scenarios such as the Harford driving cycle and *Acc* test show the limitations of NMC battery to operate at such high C-rates, given the more demanding $(P/E)_B$ requirements. The rate of discharge for the Harford and *Acc* test is in the order of 4 and 3 min, respectively. NCA can handle these rates of discharge at the price of a significant decrease of specific energy. From Fig. 3a one can calculate that the specific energy of NCA cells decreases has the C-rate goes from C/20 to 5C. In particular, there is a drop in specific energy from C/20 (256.6 $[Wh/kg]$) to 5C (18.2 $[Wh/kg]$) of about 90% at 25 °C. Conversely, LFP can be discharged under these high C-rates without showing a significant reduction in the retained specific energy. Under *Acc* test, NCA cells can only provide two-thirds of specific energy and specific power when compared to the LFP cells.A significant cell surface temperature increase occurs when the cells sustain higher C-rate cycles. As observed in Ref. [27], LFP cells have higher temperature robustness across all C-rates, as opposed to NCA and NMC, which, on the other hand, have an increase of internal heat loss proportional to the C-rate at which they are operated. A possible way to alleviate the electrical and the thermal stresses on the batteries when operated at high C-rate is to resort to HESS, where the SCs can handle the high peaks of current.

In the analysis that follows, we compute the overall mass, Fig. 11a, and energy, Fig. 11b, of the battery pack required to satisfy different load requirements. We compare the NCA and LFP batteries over *Range2*, UDDS, US06, Harford and *Acc* tests for $\alpha = 1$. As α varies between 0.5 and 1, variations in the calculated mass and energy are also provided. Strong dependency of battery sizing with respect to vehicle application clearly emerges. The increase in vehicle weight - from TMS to TST - is reflected on greater mass and energy requirements to the battery pack, independently of the selected driving scenario and energy storage type. Moreover, as the P/E ratio increases - going from *Range2* to *Acc* test - battery sizing turns out to be more sensitive to variation of α.

Fig. 11a shows that to minimize the required pack weight

[5] Such a configuration is obtained by properly set the frequency-segmentation algorithm, as indicated in Table 1.

Table 3
Driving cycle scenarios - *Range* tests at different speeds, *Acc* test, UDDS, US06 and Harford - for each vehicle application.

Driving cycle scenarios		TMS	HMMWV	TST
Constant speed over fixed mile range (*Range* test)	*Range1*: 20 mph *Range2*: 45 mph *Range3*: 70 mph	370 miles	370 miles	500 miles
Acceleration 0–60 mph (*Acc* test)		3.7 s	3.7 s	20 s
UDDS US06 Harford		Repeated until 200 miles range reached		

Table 4
Driving characteristics of the UDDS, US06 and Harford cycles.

	UDDS	US06	Harford
Average speed [mph]	19.27	47.4	36.62
Maximum speed [mph]	56.7	80.2	49.9
Average acceleration [m/s^2]	0.31	0.65	0.38
Maximum acceleration [m/s^2]	1.46	3.24	10.9
Average road grade [%]	0	0	0.14
Maximum road grade [%]	0	0	33.82

needed to satisfy high energy demanding cycles - *Range* test, UDDS and US06 - cell chemistry with improved specific energy performance, like NCA, are preferred over LFP, with a resulting weight for NCA battery pack half of that from LFP pack (for all the three vehicles). Conversely, when higher C-rates of operation are required, the high specific power chemistry is preferred, both in terms of overall mass and energy requirements.

As an exception, our analysis shows that for the military Harford cycle, the NCA and LFP pack design returns the same mass value. Finally, for the *Acc.* test, which is on the right hand spectrum of the cycle aggressiveness scale, LFP is always a better choice than NCA chemistry across all vehicles.

Simulations conducted over UDDS and US06 are used to produce bounds on the battery pack sizing. Ranges of estimated NCA battery pack weight, volume, number of cells and energy for each vehicle are shown in Table 5.

The actual battery pack of TMS is composed of 7104 NCA cells (corresponding to a mass of 337.3 kg and volume of 12 m^3), 544.2 kg total pack weight (including all the pack components) and stores 85 kWh energy [47]. Those numbers are consistent with the estimated bounds established in this paper and shown in Table 5. Similar outcome is obtained for TST vehicle, whose actual battery pack energy is claimed to be approximately 1 MWh [48].

4.2. Hybrid configuration

In this section, we analyze the case of hybrid powertrain containing an ICE, a battery pack and a SC pack for the (i) TMS tested over US06, referred to as *Scenario1* and (ii) Military HMMWV tested over Harford, referred to as *Scenario2*. The baseline case of each scenario is given when setting the tunable parameters, $f_{cut,1}$, $f_{cut,2}$ and α, as

$$\overline{f_{cut,1}} = 0.025 \text{ Hz}\,, \quad \overline{f_{cut,2}} = 1 \text{ Hz} \quad \text{and} \quad \overline{\alpha} = 1, \tag{18}$$

The corresponding battery and SC pack energy returned from the segmentation process is indicated with $\overline{E_{pack,B}}$ and $\overline{E_{pack,SC}}$, respectively.Fig. 12a and b show the power at the wheel and the segmented power among the ICE, battery and SC with respect to time, whereas Figs. 12c and d display the segmented power obtained through fast Fourier transform for *Scenario*1 and *Scenario*2, respectively.

The P/E ratios computed for each storage device and scenarios are listed in Table 6.

In the case of *Scenario1*, the calculated $(P/E)_{SC}$ value is much lower - in the order of hours-than the standard SC characteristics indicating an operating rate significantly longer than what one

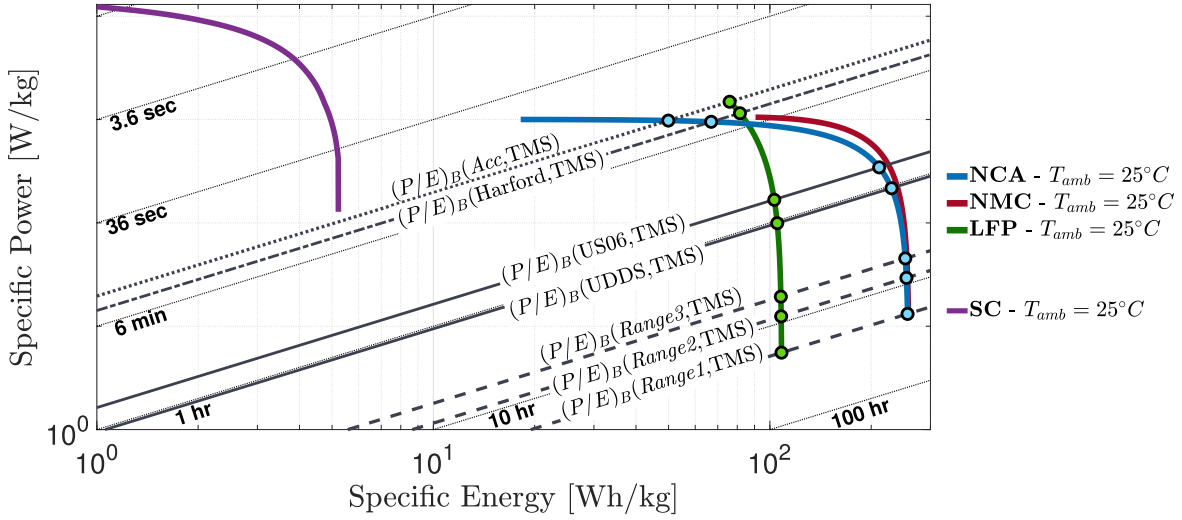

Fig. 10. ERp populated with data from NCA, NMC and LFP batteries and SC at 25°C. The $(P/E)_B$ diagonal lines are calculated for the case of TMS vehicle tested over all the driving scenarios for α set to 1. Light blue and green circle markers indicate the intersections of $(P/E)_B$ diagonal lines with the NCA and LFP curves, respectively. (For interpretation of the references to colour in this figure legend, the reader is referred to the Web version of this article.)

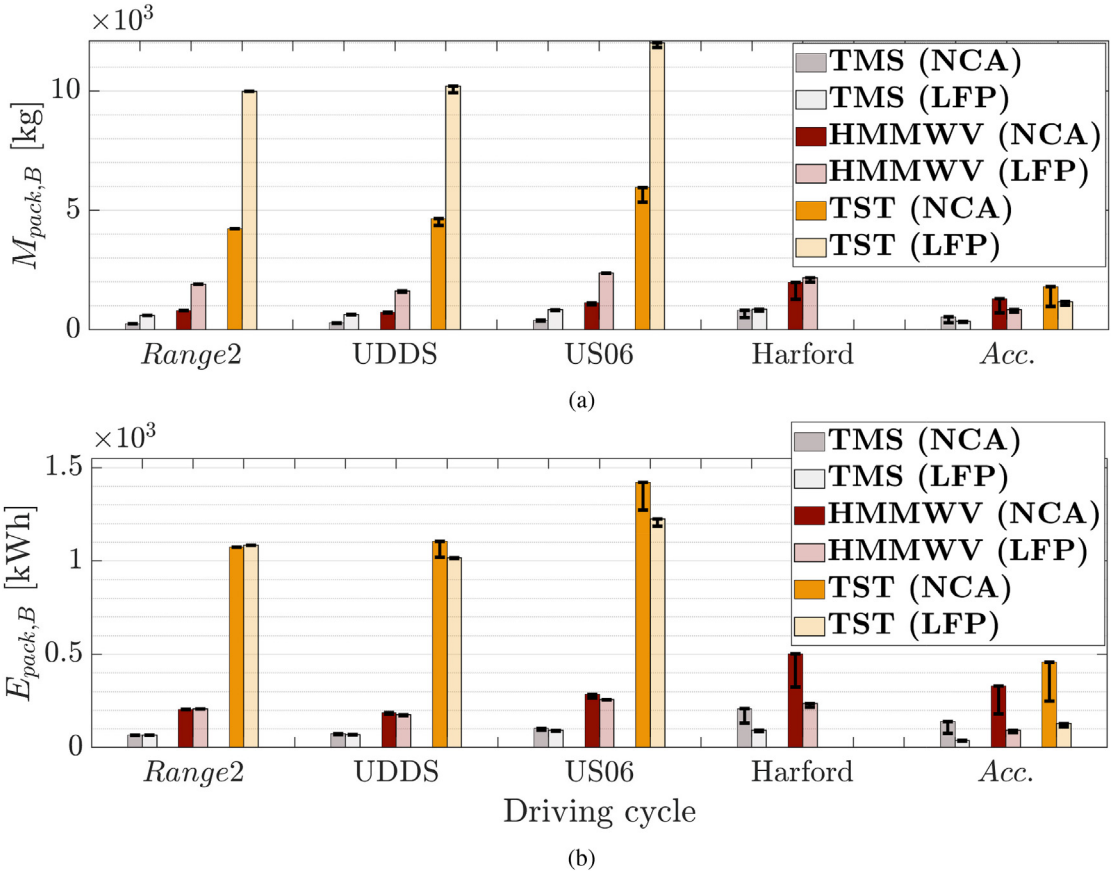

Fig. 11. Comparison between NCA and LFP battery pack sizing - in terms of (a) overall weight and (b) energy - for all vehicle applications tested over *Range2*, UDDS, US06, Harford and *Acc* driving scenarios. Each bar is obtained for $\alpha = 1$ and the variation of mass and energy as α varies from 0.5 to 1 is described by the black error bar. For ease of graphical representation, the results related to the Harford driving scenario performed with TST are not shown but only summarized here for $\alpha = 1$: $13.32 \cdot 10^3$ kg, $3.39 \cdot 10^3$ kWh when using NCA, and $12.89 \cdot 10^3$ kg and $2.24 \cdot 10^3$ kWh when using LFP chemistry instead.

Table 5
Range of estimated battery pack weight and volume (when no wiring, sensors and external case are considered), number of cells and energy for each vehicle application using NCA. The lower bounds are computed by running the UDDS cycle for $\alpha = 0.5$ and the upper bounds are calculated from the US06 for $\alpha = 1$.

Vehicle	Weight [kg]	Volume [m^3]	Number of cells [−]	Energy [kWh]
TMS	273.4–406.4	$9.7 \cdot 10^{-3}$ - $14.5 \cdot 10^{-3}$	5756–8554	69.3–103.2
HMMWV	703.6–1122	$24.9 \cdot 10^{-3}$ - $39.9 \cdot 10^{-3}$	14812–23615	178.6–284.8
TST	4014–5596	$155.2 \cdot 10^{-3}$ - $211.6 \cdot 10^{-3}$	84505–117810	1019–1421

would typically expect from a SC (in the order of seconds to minutes). Such a low $(P/E)_{SC}$ ratio value is related to the simulation scenario. In facts, the peaks of power required at the wheel always occur at low or medium frequencies (up to 0.08 Hz).

On the other hand, under *Scenario2* there is a noticeable difference between $(P/E)_B$ and $(P/E)_{SC}$. The high frequency content found in *Scenario2* is due to the heavy vehicle weight (almost two and a half times heavier than TMS) and the aggressive accelerations on a non-negligible road grade cycle. The high harmonics found in the power spectrum make the SC the perfect device to match such a $(P/E)_{SC}$. In the ERp of Fig. 13a and b, we include a sensitivity analysis of the P/E ratio for the battery and SC with respect to the cutoff frequencies, $f_{cut,1}$ and $f_{cut,2}$, under *Scenario1* and *Scenario2*. The $(P/E)_B$ and $(P/E)_{SC}$ are varied from their baseline values - the yellow and light blue solid diagonal lines, respectively - upon changes to the segmentation cutoff frequencies between the values of $5 \cdot 10^{-7}$ Hz and $5 \cdot 10^{-1}$ Hz for $f_{cut,1}$, and $5 \cdot 10^{-3}$ and 5 Hz for $f_{cut,2}$.

As shown in Fig. 13a, the variation in the cutoff frequencies still show that the $(P/E)_{SC}$ from *Scenario1* is inconsistent with SC characteristics. For *Scenario2*, the values of $(P/E)_B$ and $(P/E)_{SC}$ obtained from the sensitivities analysis (Fig. 13b) show that NCA and SC characteristics can always match such requirements.

For *Scenario1*, the low demanded $(P/E)_B$ ratio calls for a LIB system with high specific energy, such as NMC, Fig. 13a which holds a minimum weight battery pack. However, to compare the design results between the hybrid and the full-electric configuration presented in the previous section, we consider a battery pack made of NCA cells. Fig. 14a shows the NCA battery pack energy as a function of the cutoff frequency $f_{cut,1}$, for values of α ranging between 0.5 and 1. As described in Table 1, the variation of $f_{cut,1}$ has an impact on the degree of vehicle electrification. Reducing $f_{cut,1}$ yields to a larger energy pack, whereas for larger $f_{cut,1}$ the vehicle "approaches" to a CV configuration. Moreover, a low α corresponds to small pack energy, resulting in up to 13.5% reduction of the pack energy with

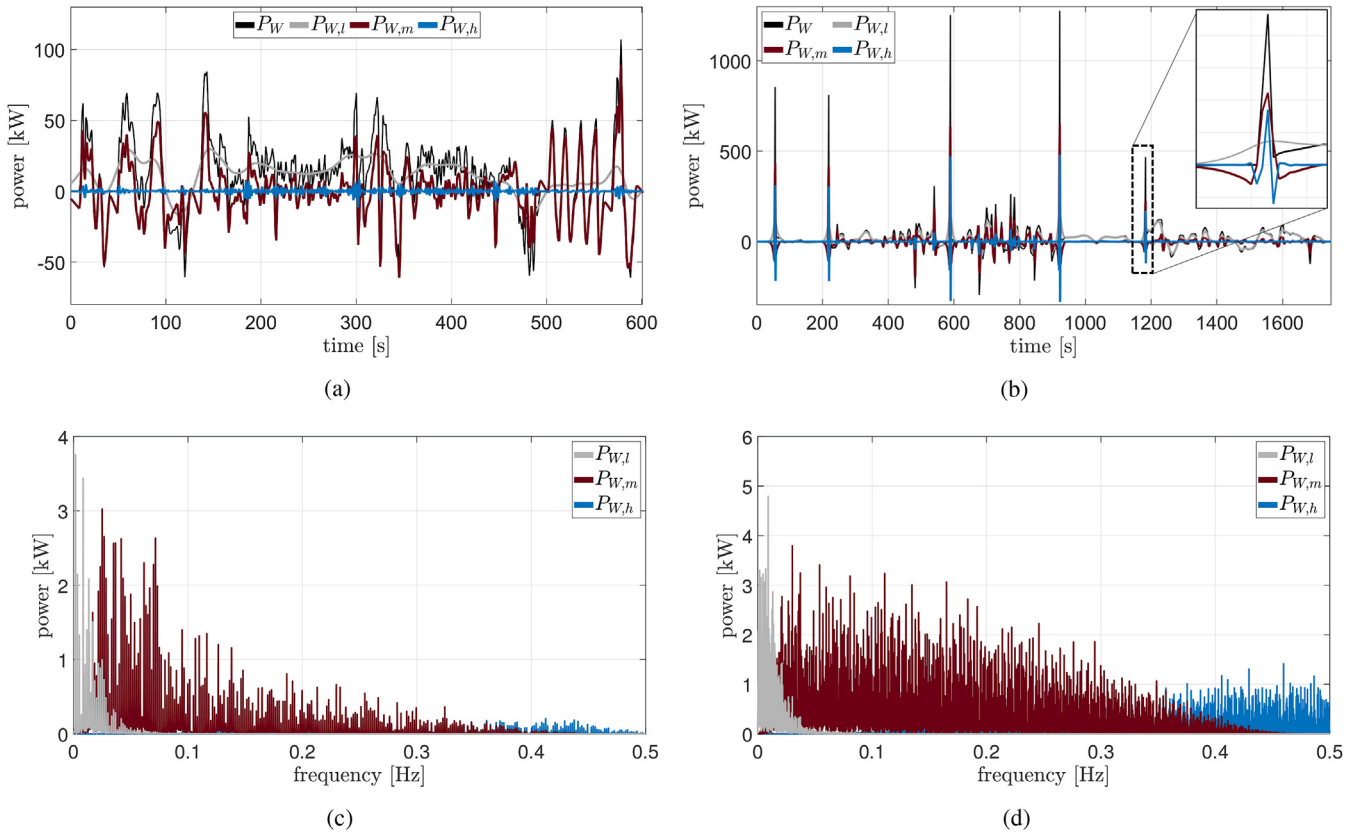

Fig. 12. Power load profile, P_W, and its segmentation in low, $P_{W,l}$, medium, $P_{W,m}$, and high, $P_{W,h}$, frequency components corresponding to ICE, battery and SC, for *Scenario1* (a) and *Scenario2* (b), and the corresponding frequency-domain components (c) and (d), respectively.

Table 6
$(P/E)_B$ and $(P/E)_{SC}$ computed for the battery and SC in each scenarios in the hybrid powertrain case.

	*Scenario*1	*Scenario*2
	US06 TMS	Harford, HMMWV
$(P/E)_B$ [1/h]	2.86	17.43
$(P/E)_{SC}$ [1/h]	2.63	54.21

respect to the baseline case when $\alpha = 0.5$. For *Scenario 2*, the sizing of both battery and SC is addressed. Fig. 14b shows the required battery and SC pack energy as a function of the cutoff frequency $f_{cut,1}$, for α between 0.5 and 1 while $f_{cut,2}$ is set to its baseline value. Differently from *Scenario1*, the P/E ratio is much higher making the $E_{pack,B}$ strongly dependent on α at low frequencies (up to 35.6% reduction compared to the baseline value). However, such a

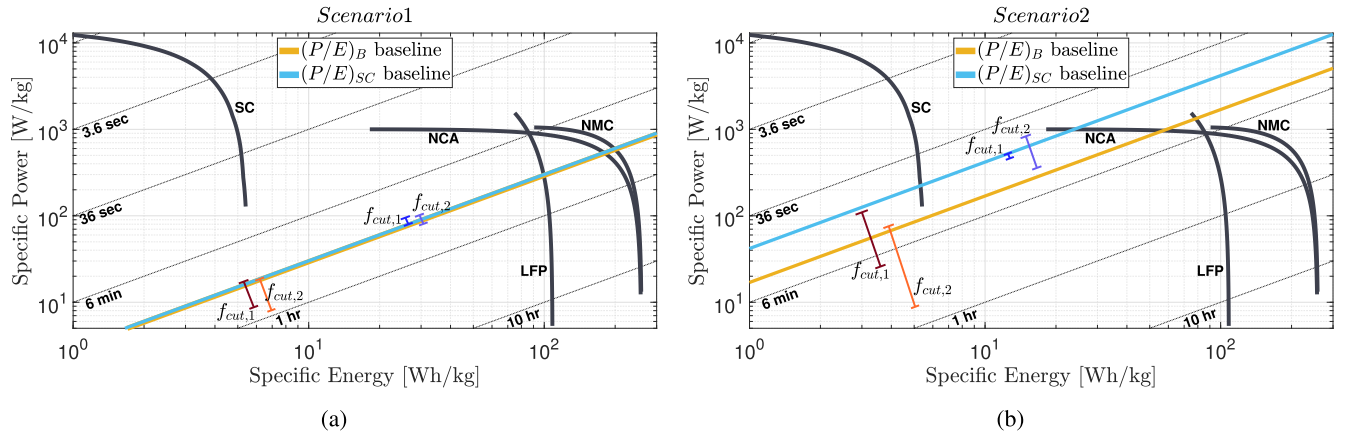

Fig. 13. ERp showing the variation of $(P/E)_B$ as function of $f_{cut,1}$ and $f_{cut,2}$, indicated with a red and orange error bars, respectively, for *Scenario1*. Blue and purple error bars are used to depict the variation of $(P/E)_{SC}$ as function of $f_{cut,1}$ and $f_{cut,2}$, respectively, for *Scenario2*. (For interpretation of the references to colour in this figure legend, the reader is referred to the Web version of this article.)

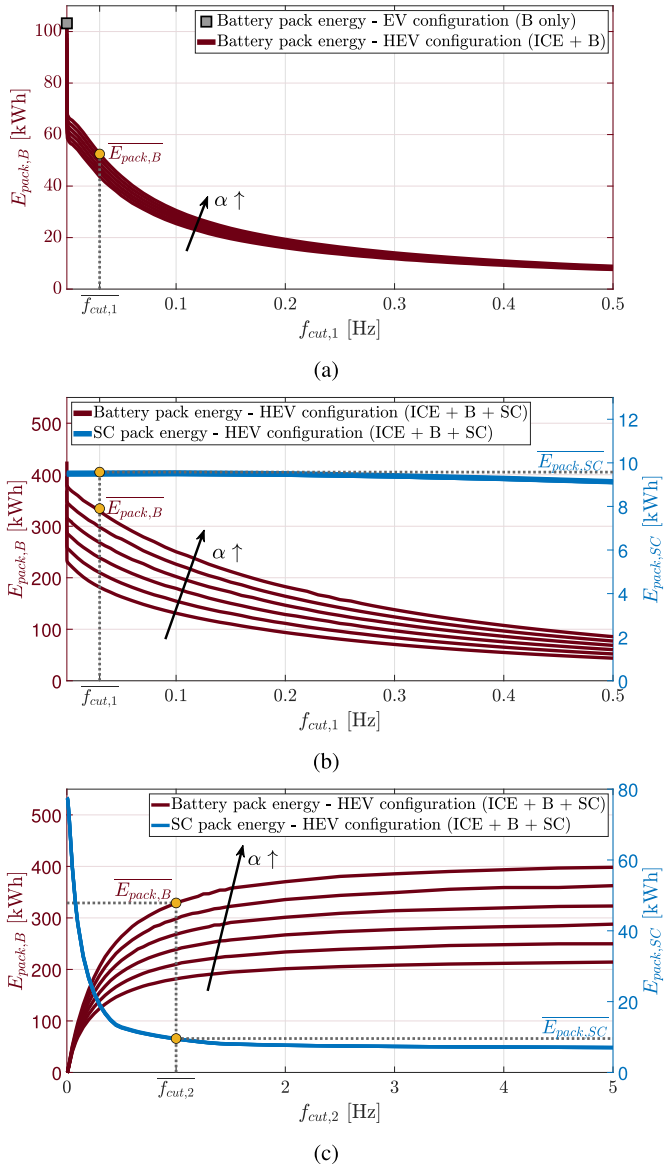

Fig. 14. (a) *Scenario1*: battery pack energy, $E_{pack,B}$, as a function of the cutoff frequency $f_{cut,1}$. The square gray marker - at $f_{cut,1} = 0$ - corresponds to the battery size in the EV configuration. *Scenario2*: battery and SC pack energy, $E_{pack,B}$ and $E_{pack,SC}$, as a function of the cutoff frequency $f_{cut,1}$ (b) and $f_{cut,2}$ (c). Results are showed for α ranging from 0.5 to 1. The battery and SC pack sizes, $\overline{E_{pack,B}}$ and $\overline{E_{pack,SC}}$ highlighted with circle yellow markers.are given for the baseline conditions - $f_{cut,1} = \overline{f_{cut,1}}$, $f_{cut,2} = \overline{f_{cut,2}}$ and $\alpha = \bar{\alpha}$. (For interpretation of the references to colour in this figure legend, the reader is referred to the Web version of this article.)

dependency is attenuated at higher $f_{cut,1}$ values. The size of SC is found to be weakly dependent on $f_{cut,1}$ ($E_{pack,SC}$ stays bounded between 9.01 and 9.57 kWh) and α (the variation of $E_{pack,SC}$ with respect to α never exceeds 6.1%, for all $f_{cut,1}$ values).

Fig. 14b shows the required battery and SC pack energy as a function of $f_{cut,2}$ and α ranging from 0.5 to 1, while $f_{cut,1}$ is set to its baseline value. The larger $f_{cut,2}$, the larger is the battery. The $E_{pack,B}$ is more sensitive to α for higher $f_{cut,2}$ (up to 47.2% variation), conversely, $E_{pack,SC}$ is not sensitive to α as $f_{cut,2}$ varies (its variation is limited to 6.25%).

One of the main disadvantages of SCs, besides the high cost, is their low volumetric energy. These are the two main factors that make them a not-market ready solution at large [49]. In the following analysis, we assess the volume occupied by each device for the case of *Scenario2*. We define the percentage relative volume, h, as the volume of the SC relative to the volume occupied by the HESS

$$h = \left(\frac{V_{pack,SC}}{V_{pack,B} + V_{pack,SC}} \right) \cdot 100. \tag{19}$$

For the baseline case, SCs account for 17.52% of the overall HESS volume.

We analyze the volume to each device and the relative volume, h, as a function of the cutoff frequency $f_{cut,1}$, Fig. 15a and c, and $f_{cut,2}$, Fig. 15b and d. The volume required to each device shows the same dependence on α that was previously established for the pack energy, for both cutoff frequencies. Consequently, the relative percent ratio h decreases as α increases (throughout the whole cutoff frequency range). From Fig. 15c one can see that the SC volume is increasing for higher values of $f_{cut,1}$, making up to 60% of the overall HESS volume for the lowest value of α. From Fig. 15d, strong dependency between the SC volume requirement and $f_{cut,2}$ is found at low frequency. Low values of $f_{cut,2}$ lead to an HESS mostly made with SCs.[6] Conversely, by increasing $f_{cut,2}$ the value of h decreases up to 10%.

5. Safety considerations

Battery packs are required to meet several automotive technical requirements, in addition to satisfy the vehicle power and energy demand [16]. The battery management system (BMS) controls and monitors the performance (temperature, current, voltage, isolation, etc.) of the battery cells during use to guarantee that the battery is working within its predetermined safety operating region. The housing of the battery pack is properly designed to be robust to mechanical stress. The thermal cooling is specifically designed with a great deal of attention to allow the battery to never experience high temperature of operation which could lead to thermal runaway. The battery pack geometry, structural design and position within the vehicle are all relevant design parameters when integrating the battery pack in the vehicle to ensure safety. Those design and control decisions that will result in a given battery topology and a properly crafted BMS are taken and developed once the cell chemistry is chosen [16], as done, for example in Ref. [50] for an eBus application. Once the chemistry is selected, the pack is design to meet packaging space constraints, and operating and safety requirements. For the three LIBs employed in this work, classification in terms of their specific energy, specific power, safety, life span and performance, can be provided [51]. For example, NCA battery is the less safe among the three. Thus, if one wants to use this chemistry - owing its higher specific energy- particular attention and care needs to be paid to design a robust thermal control management unit around it. This is the case of Tesla Model S, for instance. In our paper, we are proposing a method to assess what chemistry or device (among LIB and SC) is most suitable for a given applications in terms of energy and power characteristics. Then, guaranteeing safety performance as well as ensuring longer life span of the selected device need to be accounted for in a later design stage [52–54].

[6] When $f_{cut,2}$ tends to zero the storage system is composed by the SC pack in standalone configuration, as previously indicated in Table 1.

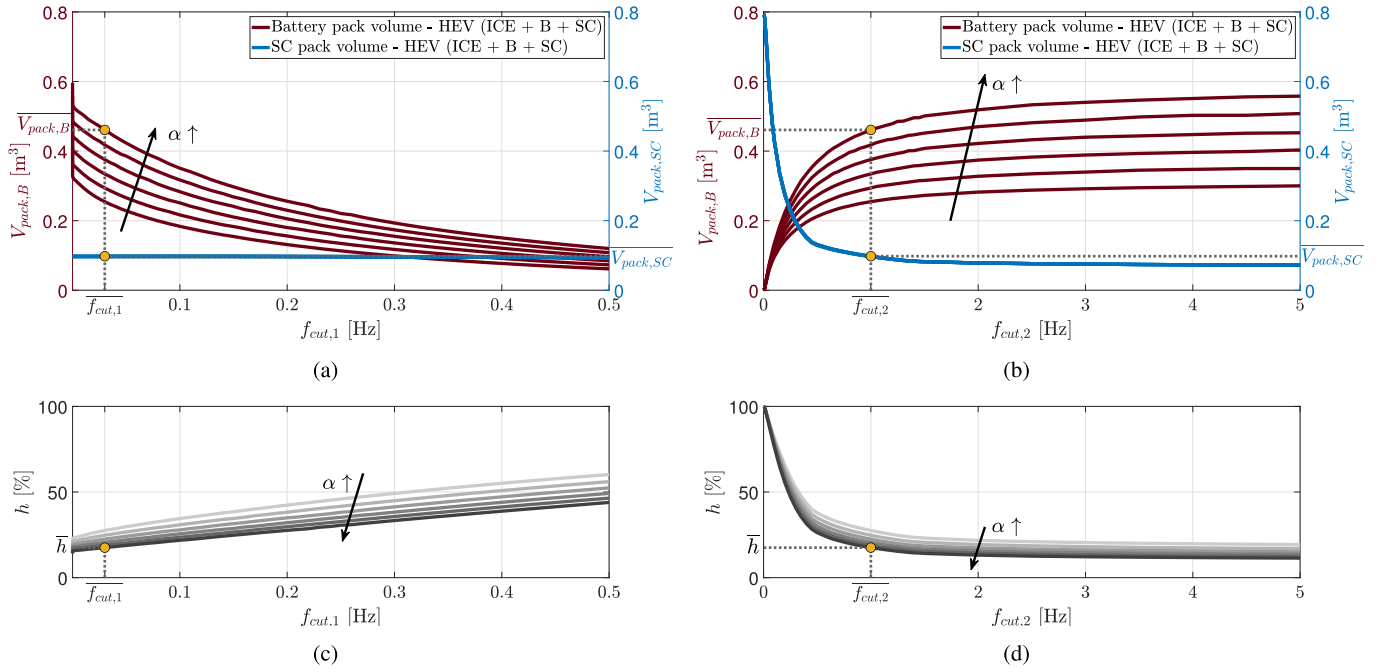

Fig. 15. The required volume of each device and the percent relative volume h are represented as a function of the cutoff frequency $f_{cut,1}$, (a) and (c) and $f_{cut,2}$, (b) and (d), respectively, as α ranges from 0.5 to 1. The yellow circle markers indicate the points related to the baseline condition. (For interpretation of the references to colour in this figure legend, the reader is referred to the Web version of this article.)

6. Conclusions

The paper presented an integrated design framework intended for the selection of the most suitable ESS for a targeted vehicle application, which relies upon the ERp to match vehicle requirements - based on vehicle characteristics and known driving cycle - with the best suitable storage technology (either in its battery standalone configuration or HESS). The framework elaborates vehicle requirements according to the P/E ratio of each powertrain actuator found using a frequency-based segmentation strategy. The matching procedure returns not only the chemistry but also the weight, volume, number of cells and energy of the device. We tested the proposed framework for full-electric battery-powered and hybrid vehicle configurations. We found that to minimize the energy storage sizing requirements needed to satisfy high energy cycles - *Range* test, UDDS and US06 - cell with higher specific energy, like NCA, are preferred over LFP. Simulation results show a pack weight reduction of 50% when NCA is used as opposed to LFP, irrespective of the vehicle type. Future investigations aim at expanding the ERp to account degradation-dependent performance to be used in the storage design and energy management studies [55,56].

Credit_author_statement

The authors contribute to the work equally.

Declaration of competing interest

The authors declare that they have no known competing financial interests or personal relationships that could have appeared to influence the work reported in this paper.

Acknowledgments

Unclassified. DISTRIBUTION STATEMENT A. Approved for public release; distribution is unlimited.This research was supported by the Automotive Research Center (ARC) at the University of Michigan, under Cooperative Agreement W56HZV-14-2-0001 with the U.S. Army Tank Automotive Research, Development, and Engineering Center (TARDEC) in Warren, MI. Disclaimer: Reference herein to any specific commercial company,product, process, or service by trade name, trademark, manufacturer, or otherwise does not necessarily constitute or imply its endorsement, recommendation, or favoring by the United States Government or the Dept. of the Army (DoA). The opinions of the authors expressed herein do not necessarily state or reflect those of the United States Government or the DoD, and shall not be used for advertising or product endorsement purposes.

References

[1] The safer affordable fuel efficient (safe) vehicles final rule for model years 2021-2026. United States Environmental Protection Agency; 2020. https://www.epa.gov/newsreleases/us-dot-and-epa-put-safety-and-american-families-first-final-rule-fuel-economy-standards.
[2] Global ev outlook 2019. IEA; 2019. https://www.iea.org/reports/global-ev-outlook-2019.
[3] Khalil G. Challenges of hybrid electric vehicles for military applications. In: 5th IEEE vehicle power and propulsion conference. VPPC '09; 2009. p. 1–3.
[4] Hodges S. Fire protection in military ground vehicles. SAE International Journal of Transportation Safety 2016;4(2):229–35.
[5] Silvas E, Hofman T, Murgovski N, Etman L, Steinbuch M, Member S. Review of optimization strategies for system-level design in hybrid electric vehicles. IEEE Trans Veh Technol 2017;66(1):57–70.
[6] Liu Z, Mamum A, Rizzo D, Onori S. Combined battery design optimization and energy management of a series hybrid military truck. SAE International Journal of Alternative Powertrains 2019;7(2):155–67.
[7] Mamun A, Liu Z, Rizzo D, Onori S. An integrated design and control optimization framework for hybrid military vehicle using lithium-ion battery and supercapacitor as energy storage devices. IEEE Transactions on Transportation Electrification 2019;5(1):239–51.
[8] Pourabdollah M, Silvas E, Murgovski N, Steinbuch M, Egardt B. "Optimal sizing of a series PHEV: comparison between convex optimization and particle swarm optimization," *4th IFAC Workshop on Engine and Powertrain Control.* Simulation and Modeling E-COSM 2015 2015;48(15):16–22.
[9] Murgovski N, Hu X, Johannesson L, Egardt B. Combined design and control

optimization of hybrid vehicles. American Cancer Society; 2015. p. 1–14.
[10] Hu X, Murgovski N, Johannesson LM, Egardt B. Comparison of three electrochemical energy buffers applied to a hybrid bus powertrain with simultaneous optimal sizing and energy management. IEEE Trans Intell Transport Syst 2014;15(3):1193–205.
[11] Ragone D. Review of battery systems for electrically powered vehicles, vol. 1. *SAE Technical Paper Series*; 1968. p. 1–8.
[12] Schupbach R, Balda J, Zolot M, Kramer B. Design methodology of a combined battery-ultracapacitor energy storage unit for vehicle power management. In: IEEE 34th annual conference on power electronics specialist, vol. 2003. PESC '03.; 2003. p. 88–93.
[13] Lopes J, Pomilio J, Ferreira P. Optimal sizing of batteries and ultracapacitors for fuel cell electric vehicles. In: IECON proceedings (industrial electronics conference), vol. 1; 2011. p. 4603–8.
[14] Zhang Y, Tang X, Qi Z, Liu Z. The Ragone plots guided sizing of hybrid storage system for taming the wind power. Int J Electr Power Energy Syst 2015;65:246–53.
[15] Christen T, Ohler C. Optimizing energy storage devices using Ragone plots. J Power Sources 2002;110(1):107–16.
[16] Pistoia G, Liaw B. Behaviour of lithium-ion batteries in electric vehicles: battery Health, performance, safety, and cost, ser. Green energy and technology. Springer International Publishing; 2018.
[17] Peseran A. Choices and requirements of batteries for EVs, HEVs, PHEVs: a CALSTART Webinar. National Renewable Energy Laboratory; 2011. https://www.nrel.gov/docs/fy11osti/51474.pdf.
[18] Hammerschmidt C. "Audi's flagship sedan a8 comes with 48v primary power system. eeNews Automotive; 2017. https://www.eenewsautomotive.com/news/audis-flagship-sedan-a8-comes-48v-primary-power-system.
[19] Hev battery testing results 2013 chevrolet malibu eco - vin 7249. Idaho National Laboratory (INL); 2014. https://www.energy.gov/sites/prod/files/2015/02/f19/batteryMalibu7249.pdf.
[20] Gladiator tactical unmanned ground vehicle. Military Wiki 2020. https://military.wikia.org/wiki/Gladiator_Tactical_Unmanned_Ground_Vehicle.
[21] E. Grabianowski, "How military robots work." Howstuffworks, https://science.howstuffworks.com/military-robot6.htm.
[22] Filipi Z, Fathy H, Hagena J, Knafl A, Ahlawat R, Liu J, Jung D, Assanis D, Peng H, Stein J. "Engine-in-the-loop testing for evaluating hybrid propulsion concepts and transient emissions - hmmwv case study. In: SAE 2006 world congress and exhibition. SAE International; 2006.
[23] M-atv. American special ops. https://www.americanspecialops.com/vehicles/m-atv/; 2020.
[24] Oshkosh family of medium tactical vehicles (fmtv). Army Technology; 2010. https://www.army-technology.com/projects/oshkosh-family-of-medium-tactical-vehicles-fmtv/.
[25] Oshkosh hemtt heavy expanded mobility tactical truck." Army Technology, https://www.army-technology.com/projects/oshkosh-hemtt/.
[26] Line haul tractor. https://asc.army.mil/web/portfolio-item/cs-css-line-haul-tractor/; 2020.
[27] Catenaro E, Rizzo M, Onori S. Experimental analysis and analytical modeling of enhanced-ragone plot. Appl Energy 2021;291:116473.
[28] "Datasheet - BC Series Ultracapacitors." Maxwell Technologies, pp. 1–5, https://www.maxwell.com/images/documents/bcseries_ds_1017105.pdf.
[29] Zolot M. Dual-source energy storage-control and performance advantages in advanced vehicles. In: Proceedings of the 20th electric vehicle symposium; 2003. https://www.semanticscholar.org/paper/Dual-Source-Energy-Storage-%E2%80%93-Control-and-Advantages/1dd28a06f37012e29dbcda21b890fad5a73e128e.
[30] Vehicle and Fuel Emissions Testing." United States Environmental Protection Agency, https://www.epa.gov/vehicle-and-fuel-emissions-testing/dynamometer-drive-schedules.
[31] Datasheet - ncr-18650b." Panasonic, https://www.imrbatteries.com/content/panasonic_ncr18650b-2.pdf.
[32] Product specification rechargeable lithium ion battery model inr21700 m50 18.20wh." LG Chem, https://dnkpower.com/wp-content/uploads/2019/02/LG-INR21700-M50-Datasheet.pdf.
[33] Nanophosphate high power lithium ion cell anr26650m1-b. A123 Systems; 2012. https://www.batteryspace.com/prod-specs/6610.pdf.
[34] Catenaro E, Onori S. Experimental data of lithium-ion batteries under galvanostatic discharge tests at different rates and temperatures of operation. Data in Brief 2021;35:106894.
[35] Onori S, Serrao L, Rizzoni G. Hybrid electric vehicles: energy management strategies. Springer; 2016.
[36] Hayes J, Goodarzi G. Electric powertrain: energy systems, power Electronics and drives for hybrid, electric and fuel cell vehicles. Wiley; 2018.
[37] Lambert F. Tesla Semi to enter first production in second half of 2020. https://electrek.co/2019/12/28/5-things-tesla-bring-market-2020/; 2019.
[38] Lambert F. Tesla Semi: elon Musk says time to bring electric trucks to volume production. https://electrek.co/2020/06/10/elon-musk-tesla-semi-electric-truck-volume-production/; 2020.
[39] Sherman D. Drag Queens: Aerodynamics Compared. Five slippery cars enter a wind tunnel; one slinks out a winner. Car and Driver; 2014. https://www.caranddriver.com/features/a15108689/drag-queens-aerodynamics-compared-comparison-test/.
[40] Tesla semi. Tesla; 2020. https://www.tesla.com/semi.
[41] Kane M. Tesla semi test Hints at towing Capacity: Video. InsideEVs; 2019. https://www.insideevs.com/news/356428/tesla-semi-tests-hints-towing-capacity/.
[42] Stenvall H. Driving resistance analysis of long haulage trucks at volvo-test methods evaluation. Ph.D. dissertation. 2010.
[43] "National research council (u.s. Transportation research board, tires and passenger vehicle fuel economy. Washington, DC: The National Academies Press; 2006.
[44] "Tesla Model S. Tesla. https://www.tesla.com/models; 2020.
[45] Tate E, Harpster M, Savagian P. The electrification of the automobile: from conventional hybrid, to plug-in hybrids, to extended-range electric vehicles. in *SAE International Journal of Passenger Cars: Electronic and Electrical Systems* 2009;1(1):156–66.
[46] Han D, Choi N, Cho S, Yang J, Kim K, Yoo W, Jeon C. Characterization of driving patterns and development of a driving cycle in a military area. Transport Res Transport Environ 2012;17(7):519–24.
[47] Pressman M. Understanding tesla's lithium-ion batteries. https://evannex.com/blogs/news/understanding-teslas-lithium-ion-batteries; 2017.
[48] Deveza C. Tesla semi's <2kWh/mile consumption hints at serious battery improvements and cost reduction. Tesmanian 2020. https://www.tesmanian.com/blogs/tesmanian-blog/tesla-semi-page-update-hints-at-massive-battery-improvements-and-cost-reduction.
[49] Le Fèvre P. The silent power of supercapacitors. Electronica-Azi International 2018. https://www.powersystemsdesign.com/articles/the-silent-power-of-supercapacitors/135/13510.
[50] S. Arora and A. Kapoor, Behaviour of lithium-ion batteries in electric vehicles: battery health, performance, safety, and cost. Green energy and technology, 02 2018, ch. Mechanical design and packaging of battery packs for electric vehicles, pp. 175–200.
[51] Rudisuela K. Competitive technologies to high nickel li-ion batteries – the pros and cons. Nickel Institute; 2020.
[52] Yw J, GunGoo L, TaeYong K, SangWon B, Cypress L, KyeongBeom C, Hanyong L, Sang C, Kiho K, Jun S. Development of battery pack design for high power li-ion battery pack of hev. World Electric Vehicle Journal 2007;1(94–99):12.
[53] Bhattacharjee A, Mohanty R, Ghosh A. Design of an optimized thermal management system for li-ion batteries under different discharging conditions. Energies 2020;13(21).
[54] Lyu Y, Siddique A, Majid S, Biglarbegian M, Gadsden S, Mahmud S. Electric vehicle battery thermal management system with thermoelectric cooling. Energy Rep 2019;5:822–7.
[55] Todeschini F, Onori S, Rizzoni G. An experimentally validated capacity degradation model for li-ion batteries in phevs applications. In: 8th IFAC symposium on fault detection, supervision and safety of technical processes 2012; 2012.
[56] Di Filippi A, Stockar S, Onori S, Canova M, Guezennec Y. Model-based life estimation of li-ion batteries in phevs using large scale vehicle simulations: an introductory study. In: IEEE vehicle power and propulsion conference; 2010.